

AD-A053 931

GENERAL MOTORS CORP INDIANAPOLIS IND DETROIT DIESEL --ETC F/6 20/4
RESEARCH ON AEROELASTIC PHENOMENA IN AIRFOIL CASCADES: AN EXPER--ETC(U)
APR 78 S FLEETER, R E RIFFEL, T H LINDSEY N00014-72-C-0351

UNCLASSIFIED

EDR-9477

NL

1 OF 1
AD
A053931



RESEARCH ON AEROELASTIC PHENOMENA IN AIRFOIL CASCADES

4

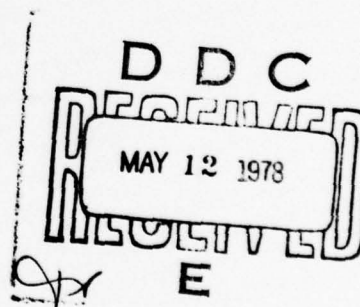
An Experimental Investigation of the Unsteady Aerodynamics of a Classical Airfoil Cascade in Translation



Cascades and Flow Systems Research

SANFORD FLEETER
RONALD E. RIFFEL
THOMAS H. LINDSEY
MARK D. ROTHROCK

APRIL 1978



AD No. 1
DDC FILE COPY

Research Supported in Part by
Office of Naval Research
Power Branch
Under Contract N00014-72-C-0351



Detroit Diesel Allison
Division of General Motors Corporation
Indianapolis, Indiana 46206

DISTRIBUTION STATEMENT A

Approved for public release;
Distribution Unlimited

An Experimental Investigation of the Unsteady Aerodynamics of a Classical Airfoil Cascade in Translation

SANFORD FLEETER
RONALD E. RIFFEL
THOMAS H. LINDSEY
MARK D. ROTHROCK

APRIL 1978

Research Supported in Part by
Office of Naval Research
Power Branch
Under Contract N00014-72-C-0351



Detroit Diesel Allison
Division of General Motors Corporation
Indianapolis, Indiana 46206

The United States government is authorized to reproduce
and distribute reprints for governmental purposes not-
withstanding any copyright notation hereon.

EDR 9477

DISTRIBUTION STATEMENT A
Approved for public release;
Distribution Unlimited

ABSTRACT

The advent of high tip-speed, high work, blading in the fan stages of advanced gas turbine engines has led to the recognition of a new type of blading instability - unstalled supersonic flutter. As a result, a concerted effort to develop an appropriate predictive mathematical model has taken place. To determine the range of validity and to direct refinements to the basic flow model, fundamental supersonic oscillating cascade data are required. The experiment described herein is directed at significantly extending the range of existing supersonic cascade data to include translation mode oscillations. In particular, the fundamental time-variant translation mode aerodynamics are determined for the first time for a classical airfoil cascade in a supersonic inlet flow field over a range of interblade phase angles at a realistic reduced frequency value. These unique experimental data are then correlated with predictions obtained from an appropriate state-of-the-art harmonically oscillating flat plate cascade aerodynamic analysis.

ACCESSION for	
NTIS	White Section <input checked="" type="checkbox"/>
DDC	Buff Section <input type="checkbox"/>
UNANNOUNCED	<input type="checkbox"/>
JUSTIFICATION	
BY	
DISTRIBUTION/AVAILABILITY CODES	
Dist.	AVAIL. and/or SPECIAL
A	

TABLE OF CONTENTS

	<u>PAGE</u>
ABSTRACT	i
NOMENCLATURE	iii
LIST OF TABLES	iv
LIST OF FIGURES	v
INTRODUCTION	1
EXPERIMENTAL FACILITY	5
AIRFOIL CASCADE AND INSTRUMENTATION	8
TRANSLATION MODE DRIVE SYSTEM	11
DATA ACQUISITION AND ANALYSIS	13
RESULTS	18
SUMMARY AND CONCLUSIONS	22
REFERENCES	24

NOMENCLATURE

C	airfoil chord
C_p	unsteady pressure coefficient ($C_p = p / \frac{1}{2} \rho U^2 \frac{h}{C}$)
M	Mach number
R_c	cascade pressure ratio
R_{xr}	normalized auto-correlation function
R_{xyr}	normalized cross-correlation function
U	inlet velocity
f	frequency
h	translational amplitude
k	reduced frequency ($k = \omega C / U$)
p	measured unsteady pressure amplitude
p_s	inlet static pressure
γ	ratio of specific heats
θ	phase lag
ρ	inlet air density
ω	angular frequency

LIST OF TABLES

	<u>PAGE</u>
Table I. Cascade Physical Parameters	27
Table II. Percent Chord Locations of the Airfoil Surface Dynamic Pressure Transducers . . .	28

LIST OF FIGURES

	<u>PAGE</u>
Figure 1. Rectilinear Cascade Facility	29
Figure 2. View of Cascade Test Section	30
Figure 3. Cascade Inlet Sidewall Bleed Strip	31
Figure 4. Schematic of Airfoil Profile	32
Figure 5. Dynamically Instrumented Airfoil	33
Figure 6. Schematic of Translation Mode Drive System . .	34
Figure 7. Translation Mode Cascade Drive System as Installed in Test Section	35
Figure 8. Periodic Steady-State Flow Field at the Inlet Mach Number of 1.40 and a Static Pressure Ratio Value of Unity	36
Figure 9. Comparison of Experimental and Predicted Overall Cascade Flow Field	37
Figure 10. Unsteady Cascade Translation Mode Results for a 2.9° Interblade Phase Angle at a Static Pressure Ratio of 1.00:1	38
Figure 11. Unsteady Cascade Translation Mode Results for a -35.0° Interblade Phase Angle at a Static Pressure Ratio of 1.00:1	39
Figure 12. Unsteady Cascade Translation Mode Results for a -41.0° Interblade Phase Angle at a Static Pressure Ratio of 1.00:1	40
Figure 13. Unsteady Cascade Translation Mode Results for a -90.0° Interblade Phase Angle at a Static Pressure Ratio of 1.00:1	41
Figure 14. Unsteady Cascade Translation Mode Results for a -178.0° Interblade Phase Angle at a Static Pressure Ratio of 1.00:1	42

	<u>PAGE</u>
Figure 15. Unsteady Cascade Translation Mode Results for a 45.0° Interblade Phase Angle at a Static Pressure Ratio of 1.30:1	43
Figure 16. Unsteady Cascade Translation Mode Results for a 0.0° Interblade Phase Angle at a Static Pressure Ratio of 1.30:1	44
Figure 17. Unsteady Cascade Translation Mode Results for a -64.0° Interblade Phase Angle at a Static Pressure Ratio of 1.30:1	45
Figure 18. Unsteady Cascade Translation Mode Results for a -90.0° Interblade Phase Angle at a Static Pressure Ratio of 1.30:1	46
Figure 19. Unsteady Cascade Translation Mode Results for a -180.0° Interblade Phase Angle at a Static Pressure Ratio of 1.30:1	47

INTRODUCTION

The advent of high tip-speed, high work, blading in the fan stages of modern gas turbine engines has led to the recognition of a new type of blading instability - supersonic unstalled flutter. In this region of instability, the incidence angle is small and the tip region of the blade row is operating in a supersonic relative flow field. The stresses encountered during this type of flutter can be catastrophically large, with all of the blade tip sections harmonically oscillating at their natural frequencies with a constant interblade phase angle. Both predominantly bending (translation) and torsional modes of vibration have been observed. As this supersonic unstalled flutter boundary crosses the compressor operating line at high tip speeds, it imposes a definite design constraint on the high speed operation of the engine and, hence, has been receiving a great deal of attention.

Unstalled supersonic flutter is fundamentally an inviscid phenomena caused by the phase lag of the flow field relative to the motion of the airfoils. As this type of flutter tends to become more severe as the pressure ratio is lowered, the generally used analytically model assumes an inviscid, essentially supersonic flow with a subsonic axial component through

a differential radial height fan stage operating at a pressure ratio of one. This differential fan stage is then developed into a two-dimensional rectilinear cascade. The cascade airfoils are assumed to be thin (most often zero thickness flat plates) and executing small harmonic torsion or translation mode oscillations. These assumptions lead to mathematical simplifications which result in a linearized, two-dimensional, constant coefficient (for the case of flat plate cascades), partial differential equation for the perturbation velocity potential. Various solution techniques have been and are currently being applied to this mathematical model.

A semi-infinite cascade with a subsonic leading edge locus was considered by Verdon⁽¹⁾ and Caruthers⁽²⁾ using finite difference techniques and by Brix and Platzer⁽³⁾ with the method of characteristics. Nagashima and Whitehead⁽⁴⁾ presented a third approach involving dipole distributions while Yates⁽⁵⁾ developed another linearized characteristics approach. These solutions are all in good agreement with each other. As a semi-infinite cascade is involved in these analyses, it is assumed therein that the asymptotic values for the unsteady pressure distributions and aerodynamic forces and moments obtained by computing the flow past a sufficient number of blades are representative of the infinite cascade.

Using Laplace transform techniques Kurosaka⁽⁶⁾ obtained a solution for an infinite cascade valid for low reduced frequency values and has recently extended these results to higher reduced frequencies⁽⁷⁾. Sisto and Ni⁽⁸⁾ using the time-marching technique and Verdon and McCune⁽⁹⁾, Verdon⁽¹⁰⁾, Goldstein⁽¹¹⁾, and Adamczyk and Goldstein⁽¹²⁾, also have considered the infinite cascade in supersonic flow with a subsonic axial component.

To determine the range of validity and direct refinements to the basic flow model, fundamental supersonic, harmonically oscillating aerodynamic cascade data are required. Such data have been obtained in the torsion mode for a single airfoil⁽¹³⁾, a classical airfoil cascade⁽¹⁴⁾, and an MCA (multiple-circular-arc) airfoil cascade⁽¹⁵⁾.

The current effort reported herein is directed at significantly extending the range of the above described supersonic cascade data by developing the necessary new experimental techniques and then obtaining relevant translation mode cascade data. In particular, the fundamental time-variant translation mode aerodynamics are determined for the first time for a classical airfoil cascade in a supersonic inlet flow field. The reduced

frequency value for this experiment is representative of that noted for bending flutter in rotors. All of the unsteady aerodynamic data are correlated with predictions obtained from a state-of-the-art harmonically oscillating flat plate cascade analysis.

EXPERIMENTAL FACILITY

The Detroit Diesel Allison rectilinear cascade facility, shown in Figure 1, was conceived and built as a research tool to evaluate the aerodynamic and aeroelastic characteristics of compressor and turbine blade sections. The facility is a continuous flow, non-return, pressure-vacuum type wind tunnel with the test section evacuated by means of two primary steam ejectors. Up to 10 lbm/sec of filtered, dried, and temperature-controlled air may be used.

The test section configuration used in this investigation is shown in Figure 2. As can be seen, the entrance flow to the test section is generated by fixed nozzle blocks yielding a Mach number of 1.30. The orientation of a wedge with respect to this nozzle exit flow specifies the test section Mach number, i.e., the shock or expansion wave generated by the wedge determines the cascade inlet conditions.

To aid in the establishment of the cascade inlet periodicity, bleed chambers are provided on the lower nozzle block, as indicated. Adjustment of the bleed rate through these chambers allows the inlet flow field to the rear (bottom) portion of the cascade to be affected. The inlet flow field to the front (upper) portion of the cascade is affected only

by the wedge position, with the first passage controlled to some extent by the splitter position. The build-up of the boundary layer in this first passage can produce area ratios such that this passage cannot be started. Hence, suction is provided along the front portion of the splitter to remove the boundary layer and start this first passage.

Active cascade inlet sidewall boundary layer control is also provided to assure the two-dimensionality of the cascade flow field. This is accomplished with the suction strip seen in Figure 3. It contains five discrete regions yet still permits the schlieren system to be utilized to view the cascade wave system.

Disturbances generated at the lower endwall run downstream of the cascade in the supersonic flow regime and thus can have no influence on the cascade performance. The upper endwall of the tunnel, on the other hand, is crucial in that it can influence the whole flow field downstream of the cascade and prevent the formation of a periodic exit flow field. The shape of this upper endwall also uniquely determines the cascade pressure ratio under started supersonic exit operating conditions. The most crucial portion of the upper endwall is in the early stage of compression. Here the flow splitter provides the capability to both bleed and

blow. The blowing capability, in conjunction with adjustments of the exit plenum pressure and the angle of the tailboard attached to the splitter, permits the setting of the streamline shape in this region and thereby sets the throttle condition to the first two channels of the cascade. The remaining problem is to not allow the cascade shock expansion system which impinges upon this tailboard to reflect back into the cascade. This is accomplished by making this upper tailboard porous with a 50% open area as well as having it open to the exit plenum pressure. This effectively produces a streamline representation of an infinite cascade at the design pressure ratio, as established in the first passage and results in a periodic exit flow field.

AIRFOIL CASCADE AND INSTRUMENTATION

The two-dimensional cascade utilized in this investigation was comprised of five double-trunnion airfoils, characterized by a 3.00 in. (7.62 cm.) span, a 3.00 in. (7.62 cm.) chord, and a 0.087 in. (0.220 cm.) maximum thickness at the 50 percent chord location. The airfoil profile, indicated schematically in Figure 4, consists of a flat suction surface and a triangular pressure surface. The cascade physical parameters are listed in Table I.

The proper steady-state aerodynamic performance instrumentation necessary to quantitatively describe the cascade flow field was provided. Sidewall static pressure taps were used to establish the cascade inlet and exit pressure distributions. This information together with schlieren flow visualization were used to establish the steady-state periodicity of the cascade.

To achieve realistic reduced frequency values, maintain a two-dimensional airfoil mode shape, and also maximize the imparted airfoil oscillatory amplitude for a given input driving power, unique airfoils fabricated from graphite/epoxy composite material were necessary. The airfoils were fabricated from a combination of pre-impregnated Kevlar cloth and graphite mat

injected with epoxy resin under pressure into a booking mold. Cloth fiber orientation was controlled to meet prescribed torsional and bending stress requirements while maintaining a low density and a high modulus of elasticity.

Hollow steel trunnions were attached to the airfoils at mid-chord. Cloth insertion and epoxy fill into the trunnions provided adequate strength at the critical airfoil-trunnion interface stress locations. Splines located on the trunnion were used to mount the airfoils into the translational drive system.

The fabrication of the airfoils from graphite/epoxy composite material necessitated the use of nonconventional instrumentation techniques. In particular, to maintain the desired overall composite material properties with no degradation of the airfoil surface contours, provisions for dynamic instrumentation were embedded in one airfoil during fabrication. This involved molding the dynamic pressure transducer lead wires into the airfoil as part of the lay-up and molding process. The ends of the lead wires were then exposed and the transducers attached. These flush-mounted Kulite LQ Series dynamic pressure transducers were staggered across the span of the airfoil on both the pressure and suction surfaces. Figure 5 shows a

view of this unique dynamically instrumented airfoil. The chordwise distribution of these transducers is identical on the airfoil pressure and suction surfaces, with their locations presented in Table II, and also schematically depicted in Figure 4.

TRANSLATION MODE DRIVE SYSTEM

A schematic of the translation mode drive system is presented in Figure 6. Since translation is movement normal to the chord, no bearing or other rigid axial restraint is necessary. The airfoil is positioned with the two flexible mounts consisting of a "squirrel cage" support which attaches to the spline on the airfoil trunnion by indexing over six grooves and attaching through a replaceable spring bar to a rigid mount. The indexing tabs ensure torsional restraint with no blade angle slippage. The airfoil trunnion splines are positioned axially on these devices by a driver arm clamped and piloted to the trunnion with an attached spacer tube which nests over the indexing tabs of the squirrel cage.

Translational excitation forces to each blade are supplied through the drive arm from the computer controlled electromagnets. Driving mechanisms are located on each airfoil trunnion so that proper excitation of the two-dimensional translational motion of the airfoil can be accomplished. Modification of the spring bars and/or mass control of the driver arm can be used for minor frequency adjustments of individual blades.

The double-trunnion airfoils and spring bar assemblies are mounted in plexiglas windows, thereby permitting schlieren flow visualization, and this complete assembly then installed in the test section, as seen in Figure 7. The computer controlled electromagnets excite the translation mode drive system at the airfoil-drive system natural frequency, thereby imparting the desired translation mode oscillation to the airfoil cascade at precisely controlled interblade phase angle values^(16,17). Strain gages mounted on the spring bar assemblies exhibit excellent sensitivity to the translational airfoil oscillations, and allow the measured strain gage signals to be converted to translational amplitudes.

DATA ACQUISITION AND ANALYSIS

With the tunnel in operation and the steady-state cascade periodicity properly established, as determined by the sidewall static pressure taps and the schlieren flow visualization, the computer controlled translation mode drive system is made operational. This results in controlled harmonic oscillations of the airfoil cascade at a prescribed frequency and interblade phase angle value. The resulting time-variant spring bar mounted strain gage and airfoil surface pressure transducer signals are digitized at rates to 100,000 points per second by a 16-channel analog-digital converter and multiplexer system, and stored on a magnetic disk. These digitized data are analyzed on-line to determine the fundamental aerodynamic characteristics of the unsteady phenomena. The parameters of interest include the amplitude of the airfoil motion and the pressure disturbance, the frequency, the interblade phase angle, and the phase difference between the unsteady pressures and the airfoil motion as characterized by the strain gage signal on the dynamically instrumented airfoil, i.e., the aerodynamic phase lag data is referenced to the motion of the dynamically instrumented center airfoil in the cascade.

The amplitude of the airfoil motion and the pressure disturbance are determined by fitting a second order least square function to the data, differentiating it, and evaluating the maximum. The pressure disturbance amplitude is then non-dimensionalized into an unsteady pressure coefficient, C_p , as defined in Equation 1:

$$C_p = \frac{P}{\frac{1}{2} \rho U^2 \frac{h}{C}} = \frac{P}{\frac{1}{2} \gamma M^2 p_s \frac{h}{C}} \quad (1)$$

where p is the measured unsteady pressure amplitude, ρ is the fluid density, U is the inlet velocity, γ is the ratio of specific heats, p_s is the inlet static pressure, and h/C is the ratio of the translational amplitude to the airfoil chord.

The frequency of the time-dependent data is determined through the autocorrelation function. This function describes the dependence on the values of the data at one time, X_i , on the values at another time, X_{i+r} . The normalized autocorrelation function, R_{xr} , is defined in series form as

$$R_{xr} = \frac{1}{N-r} \sum_{i=1}^{N-r} X_i X_{i+r} \bigg/ \frac{1}{N} \sum_{i=1}^N X_i X_i \quad r=0,1,2 \dots m \quad (2)$$

where:

$$X_i = X(i \Delta t)$$

$$r = \text{lag number}$$

$$N = \text{total number of dynamic data points}$$

$$m = \text{number of lags.}$$

The lag time, Δt , is inversely proportional to the rate at which the data is digitized. A typical autocorrelogram of the digitized data exhibits the features of a sine wave plus random noise. A second order least square function is fit to the data in the second positive peak of the autocorrelogram. The inverse of the time at which this least square function is a maximum is equal to the frequency, f , of the time-dependent data.

The phase difference of the pressure disturbance along the airfoil chord in relation to the airfoil motion is calculated through the cross-correlation function. This function, for two sets of data, X_i , Y_i , describes the dependence of the values of one set of data on the other. The normalized cross-correlation function, R_{xyr} , is defined as:

$$R_{xyr} = \frac{1}{N-r} \sum_{i=1}^{N-r} X_i Y_{i+r} \bigg/ \frac{1}{N} \sum_{i=1}^N X_i Y_i \quad r = -m, \dots, -1, 0, 1, \dots \quad (3)$$

where the variables are defined analogous to those in Equation (2).

As in the frequency calculation, a second order least square function is fit to the data in the first positive peak of the cross-correlogram. The time, t_p , at which this least square function is a maximum is analytically determined. The phase difference, in degrees, is calculated as

$$\theta_p = t_p f 360 \quad (4)$$

where f is the frequency calculated for the airfoil motion from the strain gage data, utilizing Equation (2).

Two sources of phase relation discrepancy are inherent in the electronic data acquisition system and correlation computation. The analog-digital (A/D) converter-multiplexer unit does not permit data to be digitized simultaneously on all channels. Consequently, an inherent phase shift is introduced into the physical data when the cross-correlation function operates on the raw digitized data. This phase shift, for the sinusoidal data in this experiment, is directly proportional to the "cut rate" of the multiplexer, as shown in Equation (5):

$$\theta_s = f_x (K_y - K_x) 360/R_a \quad (5)$$

where θ_s is the AD phase shift inherent in the computation between channels K_y and K_x , representing the respective data, Y_i and X_i . The frequency, f_x , corresponds to the disturbance in channel K_x , and R_a is the rate at which the data were being digitized.

Prior to acquiring data the electronic data acquisition system is calibrated for phase shift, θ_a , using the A/D converter and the computation described in the foregoing. Therefore, the phase difference of the pressure disturbance along the airfoil surface in relation to the airfoil motion is

$$\theta_{xy} = \theta_p - \theta_s - \theta_a . \quad (6)$$

This computational procedure results in a valid on-line data analysis system and provides the experimentalist with meaningful information with which to make judicious decisions during the test. All analyzed results are stored on a magnetic disk for further examination.

RESULTS

The procedure followed in this experiment included first obtaining a periodic steady-state cascade flow field, as determined from the schlieren flow visualization and the sidewall static pressures immediately upstream of the leading edge of each airfoil in the cascade. Figure 8 presents a schlieren photograph which typifies the periodic steady-state cascade flow field established at the inlet Mach number of 1.40 and a cascade static pressure ratio to unity. As indicated, the bow shock intersects the suction surface of the adjacent airfoil near the trailing edge, with both the reflection of this shock and the trailing edge wake shock from the adjacent airfoil intersecting the pressure surface near mid-chord. A comparison of this overall cascade steady flow field, as characterized by the location of the shock waves, with that predicted by the analysis of reference 18, is presented in Figure 9. As can be seen, the correlation between the experimentally determined shock waves and those indicated by the predicted constant pressure lines is quite good.

With the steady-state periodicity established and the cascade performance determined, the airfoil cascade was harmonically oscillated in a translation mode at a reduced frequency value

equal to 0.41. Specified interblade phase angles were investigated and at selected points, the cascade static pressure ratio increased from the nominal 1.00:1 to 1.30:1. Fundamental time-variant data were then obtained and analyzed. In addition, data obtained as part of the Independent Research and Development Program are also included herein to yield definitive data trend information. These unique translation mode data were then correlated with predictions obtained from the current state-of-the-art cascade analysis of reference 2. This analysis assumes small perturbations which are generated by oscillating zero thickness flat plate cascaded airfoils in a uniform inviscid steady flow field and includes the effect of variable blade-to-blade amplitude of oscillation, accomplished through input of the measured amplitudes into the analysis.

These unique chordwise pressure and suction surface translation mode data together with the corresponding predictions are presented herein in the form of an aerodynamic phase lag as referenced to the motion of the instrumented airfoil (the center airfoil in the cascade), and the unsteady pressure coefficient, C_p . These results for interblade phase angles between -180° and $+3^\circ$ at a cascade static pressure ratio equal to 1.00:1 are presented in Figures 10 through 14 and for interblade phase angles between -180° and $+45^\circ$ at a 1.30:1 static pressure ratio in Figures 15 through 19.

The time-variant suction surface data are seen to generally exhibit very good correlation with the predictions. The aerodynamic phase lag and unsteady pressure coefficient data are both nearly constant in the chordwise direction, with the theory predicting an approximate 60° greater lag than characteristic of the data. As the effects of increased cascade static pressure ratio are largely taken up in the trailing edge wave system, only the trailing edge of the suction surface should be affected. Indeed this is the case, as evidenced through comparison of the 1.00:1 and 1.30:1 pressure ratio suction surface data at corresponding inter-blade phase angle values, e.g. Figures 10 and 16, 13 and 18, and 14 and 19. As seen from these figures, only the suction surface phase lag and dynamic pressure coefficient data near to the trailing edge are affected as the pressure ratio is increased. However, the 1.00:1 suction surface phase lag data appears much more regular in the chordwise direction than does the corresponding 1.30:1 data.

The time-variant pressure surface data also generally exhibit very good correlation with the theoretical predictions. Both the aerodynamic phase lag and dynamic pressure coefficient data and prediction remain nearly constant in the

chordwise direction between the leading edge and the mid-chord region shock wave intersection location on this surface. The theory predicts this intersection location to be at approximately 70% of the chord, with the 1.00:1 pressure ratio data indicating the presence of a shock in the region between the 60% and 75% chord transducer locations. Comparison of the 1.00:1 and the 1.30:1 pressure ratio data indicates that the effect of increasing the back pressure is to move the shock intersection location forward on the pressure surface such that at the higher pressure ratio it lies between the 40% and 60% chord transducer locations.

An interesting trend can also be noted in the aerodynamic phase lag data-theory correlation on the pressure surface in the region between the leading edge and the shock intersection for both values of the pressure ratio which were investigated. In particular, in this region, as the interblade phase angle is decreased and attains larger negative values, the phase lag data decreases as compared to the prediction, with the best data-theory correlation obtained at a 0° interblade phase angle value.

SUMMARY AND CONCLUSIONS

An unsteady cascade experiment directed at providing fundamental translation mode aerodynamic data for the first time has been described. This data was obtained at a realistic value of the reduced frequency and is necessary for the verification and/or direction of refinements to the basic analytical model of unstalled flutter in fans and compressors. In particular, a unique dynamically instrumented classical airfoil cascade fabricated from graphite/epoxy composite material was investigated at an inlet Mach number of 1.40 over a range of interblade phase angles for two levels of aerodynamic loading. This time-variant data was then correlated with corresponding predictions obtained from a state-of-the-art unsteady cascade analysis.

The data generally exhibited very good correlation with the prediction on both the pressure and suction surfaces. The predicted suction surface phase lag was increased on the order of 60° as compared to the data, although in excellent agreement trendwise. Also, the mid-chord region pressure surface shock wave intersection location was in general agreement with the prediction for the lower pressure ratio data, but not for the higher pressure ratio as the theory does not

include the effect of back pressure. Also, in the region between the leading edge and the mid-chord region shock intersection location on the pressure surface, decreasing the interblade phase angle toward large negative values resulted in decreasing values of the phase lag data as compared to the prediction, with the best correlation obtained at the 0° interblade phase angle value.

REFERENCES

1. Verdon, J. M., "The Unsteady Aerodynamics of a Finite Supersonic Cascade with Subsonic Axial Flow", Journal of Applied Mechanics, September 1973.
2. Caruthers, J. E., "Theoretical Analysis of Unsteady Supersonic Flow Around Harmonically Oscillating Turbofan Cascades", Ph.D. Thesis, Georgia Tech, September 1976.
3. Brix, C. W., Jr. and Platzer, M. F., "Theoretical Investigation of Supersonic Flow Past Oscillating Cascades with Subsonic Leading Edge Locus", AIAA Paper No. 74-14, 1974.
4. Nagashima, T. and Whitehead, D. S., "Aerodynamic Forces and Moments for Vibrating Supersonic Cascade Blades", CUED/A-Turbo/TR59, 1974.
5. Yates, J. E., "Analysis of Supersonic Unsteady Cascades with the Method of Characteristics", AFFDL-TR-75-159, December 1975.
6. Kurosaka, M., "On the Unsteady Supersonic Cascade with a Subsonic Leading Edge - An Exact First Order Theory", ASME Journal of Engineering for Power, January 1974.
7. Kurosaka, M., "Supersonic Cascade Study", Work Currently Performed for the Air Force Office of Scientific Research.

8. Sisto, F. and Ni, R. H., "Numerical Computation of Non-stationary Aerodynamics of Flat Plate Cascades in Compressible Flow", ASME Journal of Engineering for Power, Vol. 98, No. 2, April 1976.
9. Verdon, J. M. and McCune, J. E., "Unsteady Supersonic Cascade in Subsonic Axial Flow", AIAA Journal, Vol. 13, No. 2, February 1975.
10. Verdon, J. M., "Further Developments in the Aerodynamic Analysis of Unsteady Supersonic Cascades", ASME Paper No. 77-GT-44, 45, 1977.
11. Goldstein, M. E., "Cascade With Subsonic Leading Edge Locus", AIAA Journal, Vol. 13, No. 8, August 1975.
12. Adamczyk, J. J. and Goldstein, M. E., "Unsteady Flow in a Supersonic Cascade with Subsonic Leading-Edge Locus", (to be published).
13. Novick, A. S., Jay, R. L., Sinnet, G. T., and Fleeter, S., "An Experimental Investigation of Unsteady Airfoil Motion in a Supersonic Stream", Unsteady Aerodynamics Vol. I and II, Edited by R. B. Kinney, Proceedings of a Symposium held at the University of Arizona, March 1975.

14. Fleeter, S., Novick, A. S., Riffel, R. E., and Caruthers, J. E., "An Experimental Investigation of the Unsteady Aerodynamics in a Controlled Oscillating Cascade", ASME Journal of Engineering for Power, Vol. 99, No. 1, January 1977.
15. Fleeter, S., and Riffel, R. E., "Aerodynamic Phenomena in an Oscillating Transonic MCA Airfoil Cascade Including Loading Effects", AGARD Conference on Unsteady Aerodynamics, AGARD CPP-227, September 1977.
16. Fleeter, S., McClure, R. B., Holtman, R. L., and Sinnet, G. T., "A Unique Supersonic Inlet Unsteady Aerodynamic Cascade Experiment", AIAA Paper No. 74-622, 1974.
17. Fleeter, S., McClure, R. B., Holtman, R. L., and Sinnet, G. T., "Supersonic Inlet Torsional Cascade Flutter", AIAA Journal of Aircraft, 1975.
18. Delaney, R. A. and Kavanagh, P., "Transonic Flow Analysis in Axial-Flow Turbomachinery Cascades by a Time-Dependent Method of Characteristics". ASME Paper No. 75-GT-8, ASME Transactions, Journal of Engineering for Power.

CHORD	3.00 IN. (7.62 CM.)
SOLIDITY	1.231
SETTING ANGLE	61.5° (1.07 RADIANS)
MAXIMUM THICKNESS/CHORD	0.029
LEADING EDGE WEDGE ANGLE	3.317° (0.058 RADIANS)
TRAILING EDGE WEDGE ANGLE	3.317° (0.058 RADIANS)
LEADING EDGE RADIUS/CHORD	0.0026

TABLE I. CASCADE PHYSICAL PARAMETERS

SUCTION AND PRESSURE SURFACE LOCATIONS

15.

25.

40.

60.

75.

85.

TABLE II. PERCENT CHORD LOCATIONS OF THE AIRFOIL
SURFACE DYNAMIC PRESSURE TRANSDUCERS

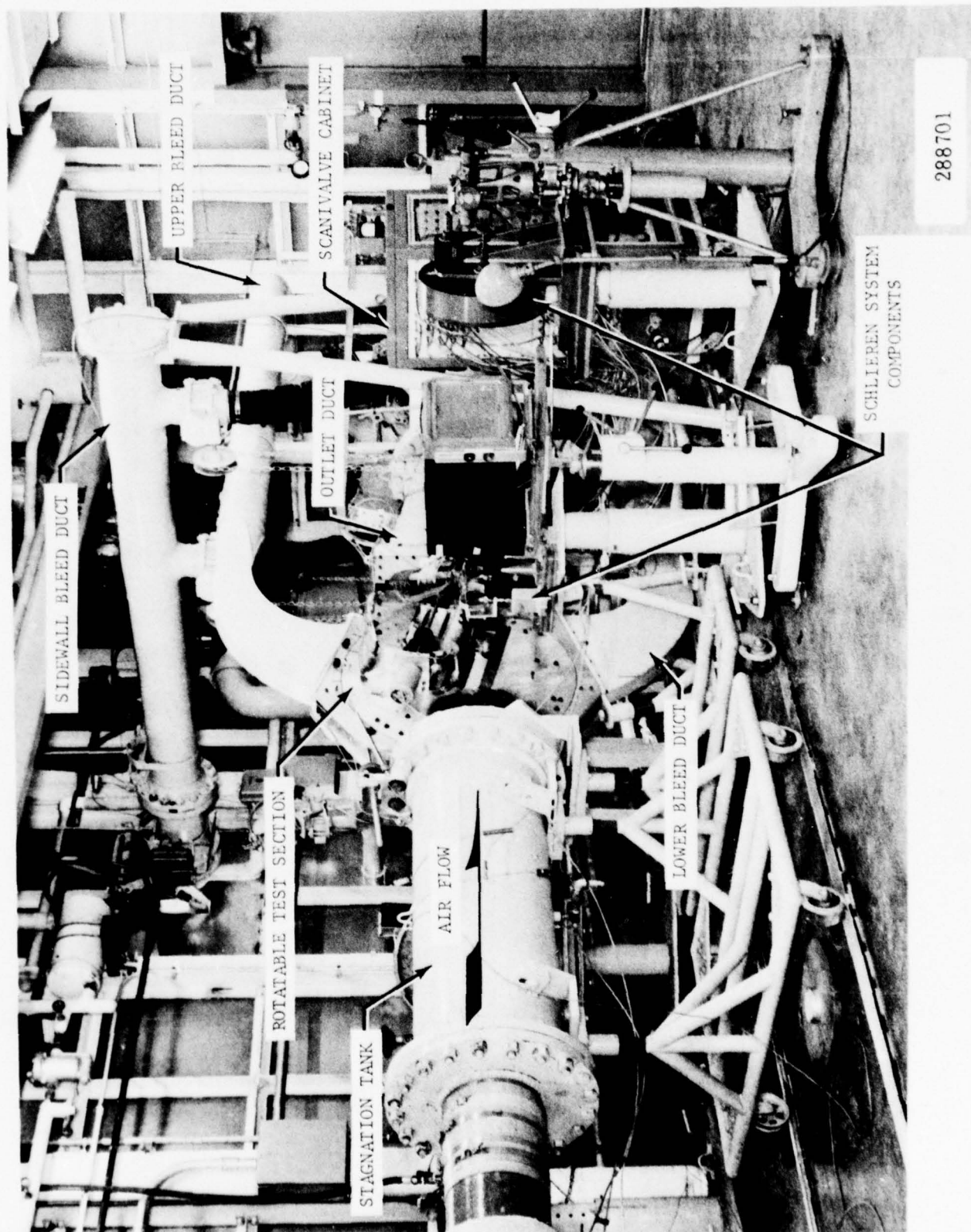


FIGURE 1. RECTILINEAR CASCADE FACILITY

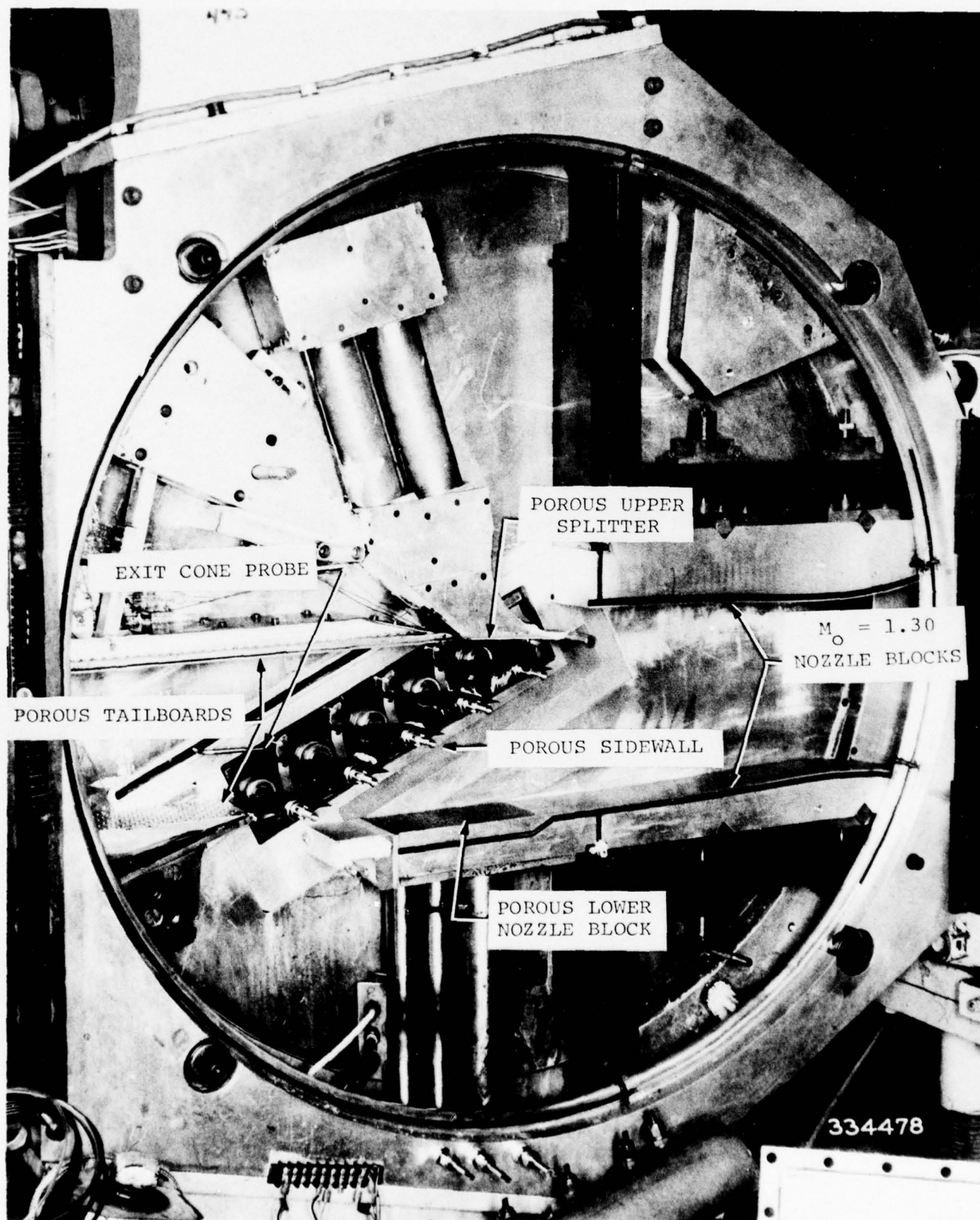


FIGURE 2. VIEW OF CASCADE TEST SECTION

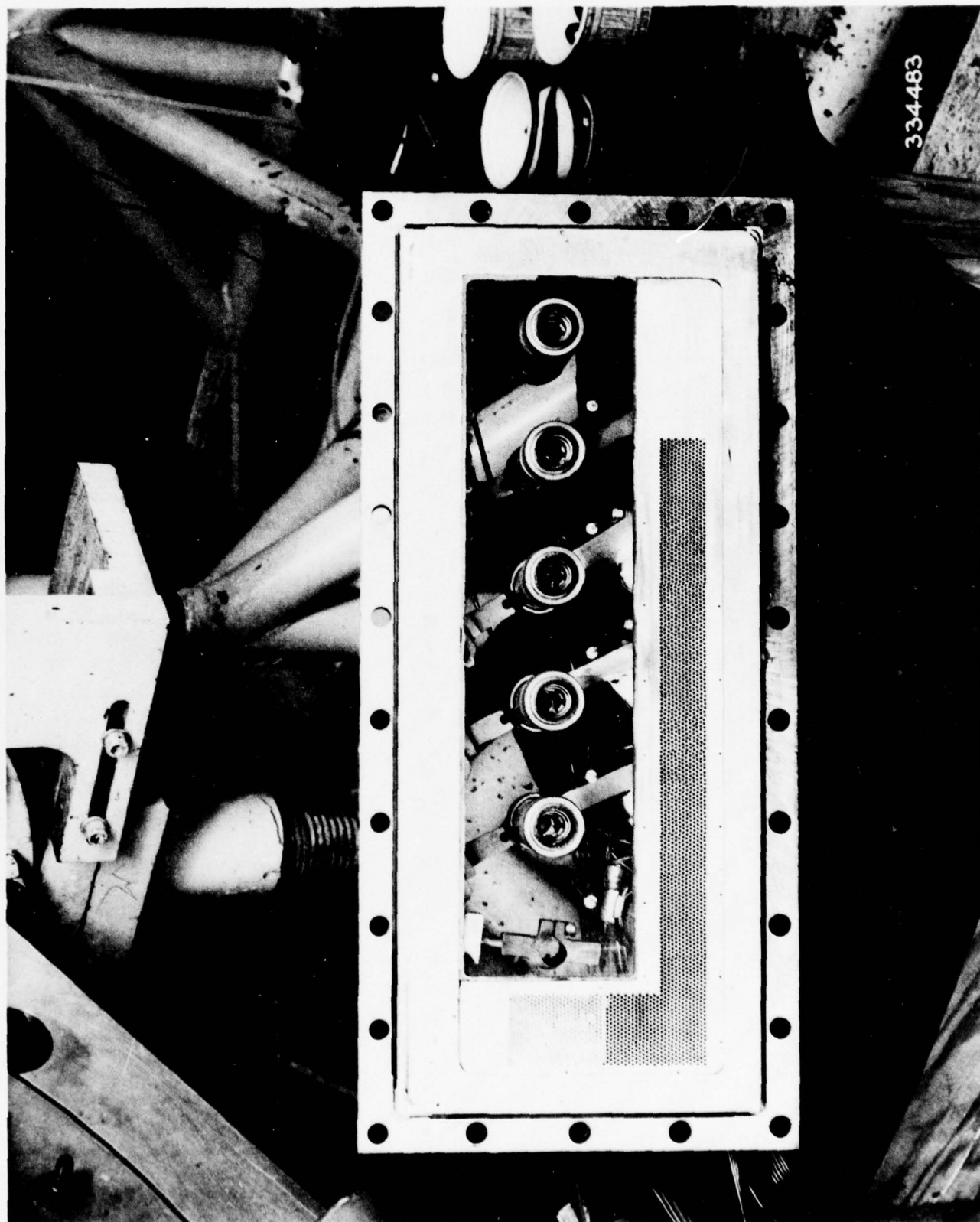


FIGURE 3. CASCADE INLET SIDEWALL BLEED STRIP



FIGURE 4. SCHEMATIC OF AIRFOIL PROFILE

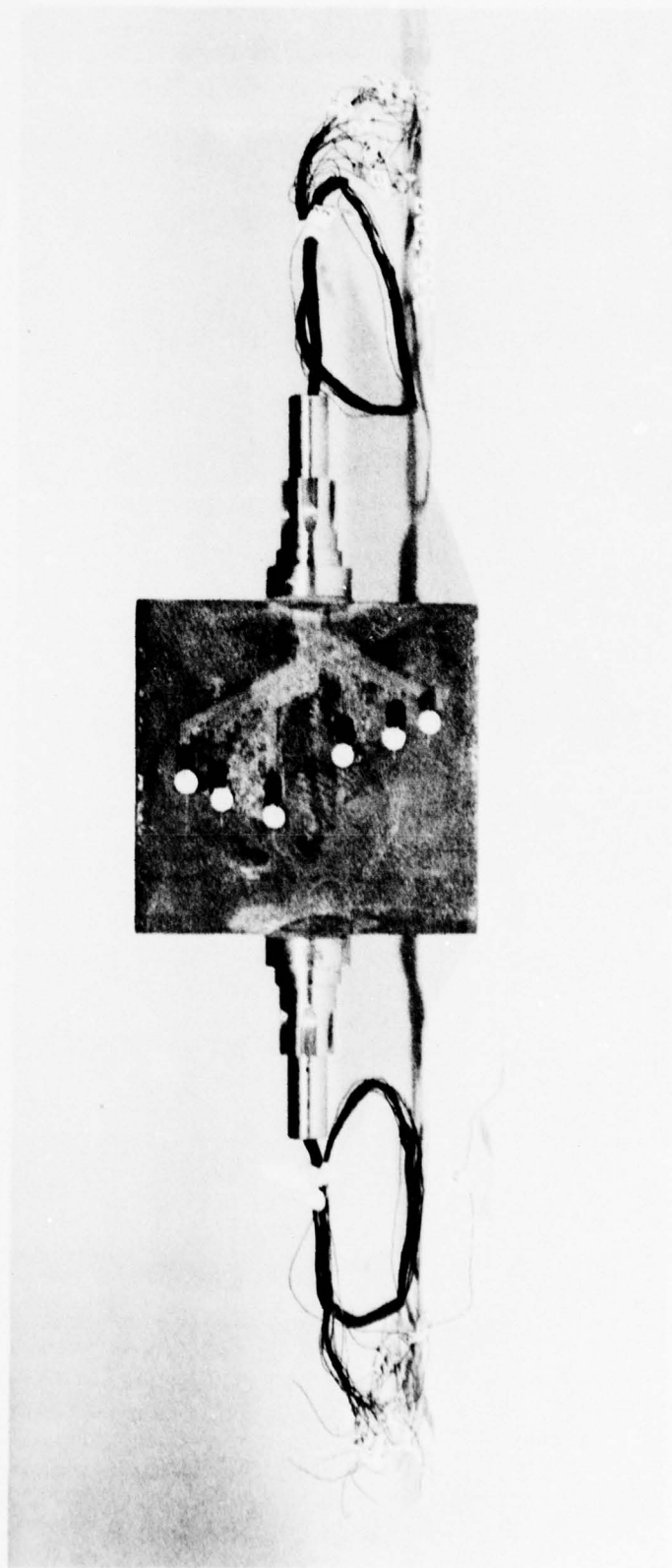


FIGURE 5. DYNAMICALLY INSTRUMENTED AIRFOIL

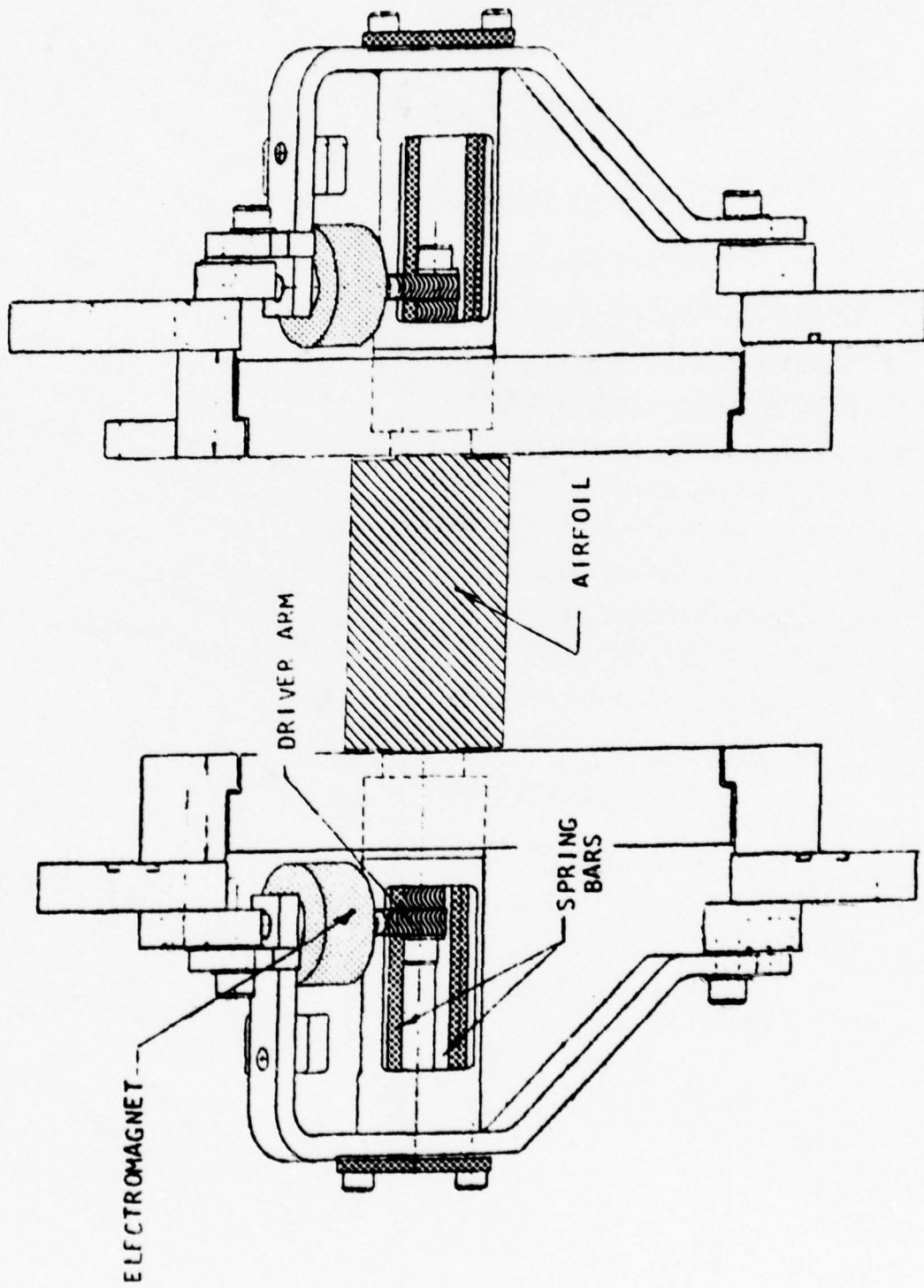


FIGURE 6. SCHEMATIC OF TRANSLATION MODE DRIVE SYSTEM

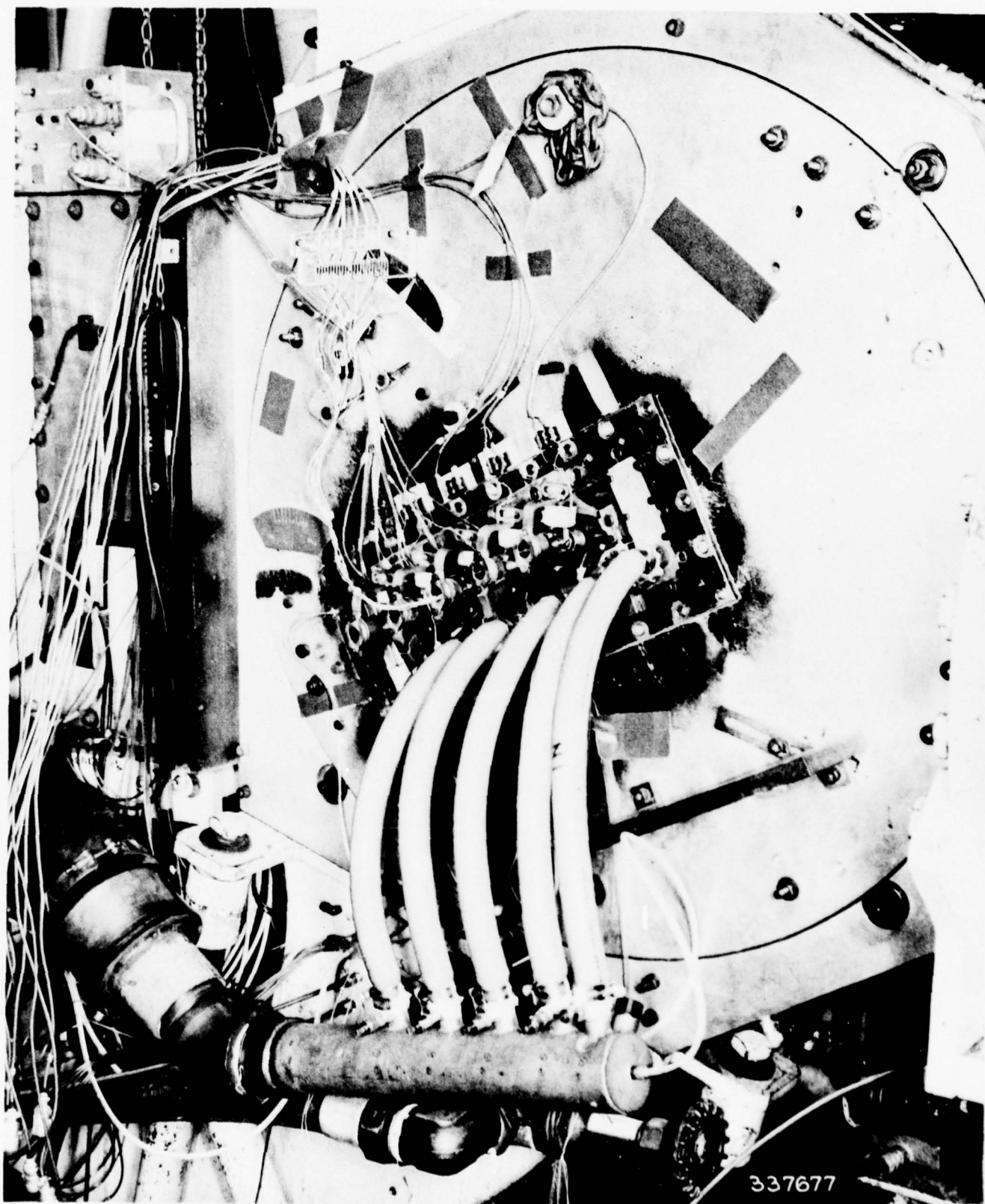


FIGURE 7. TRANSLATION MODE CASCADE DRIVE SYSTEM
AS INSTALLED IN TEST SECTION



FIGURE 8. PERIODIC STEADY-STATE FLOW FIELD AT THE INLET MACH NUMBER OF 1.40 AND A STATIC PRESSURE RATIO VALUE OF UNITY

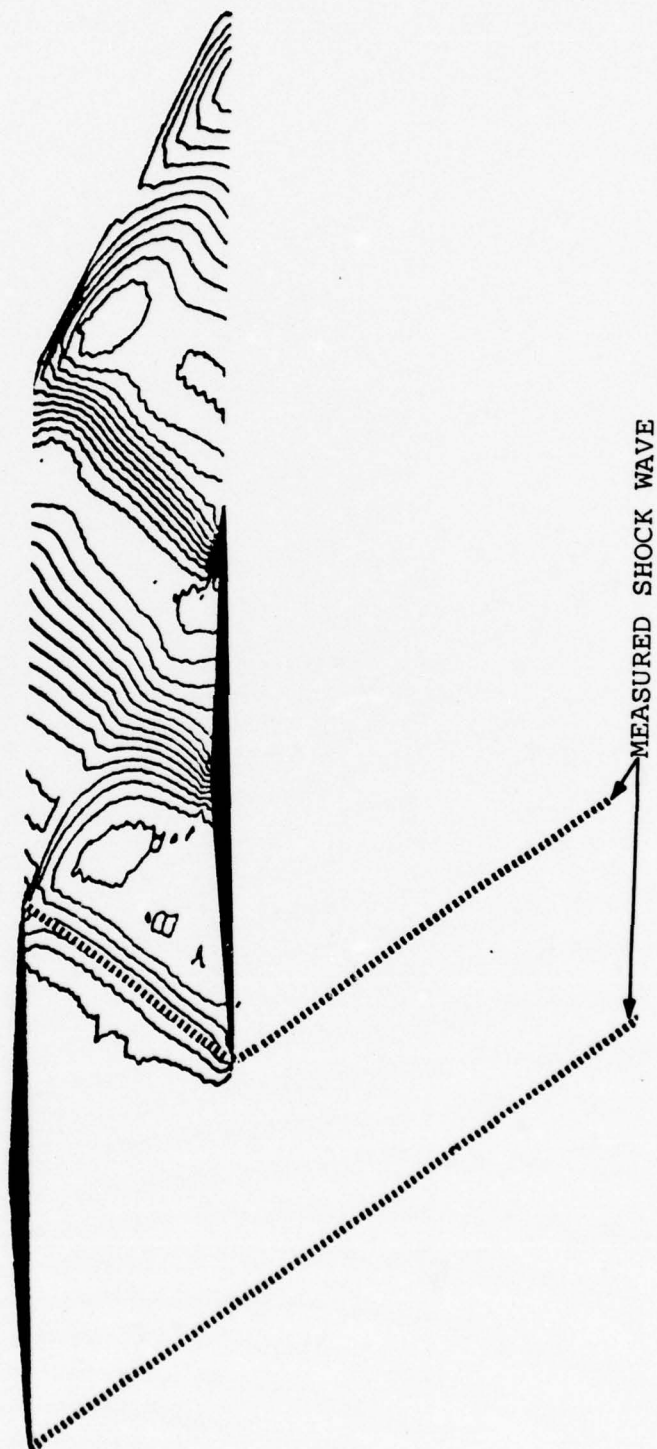


FIGURE 9. COMPARISON OF EXPERIMENTAL AND PREDICTED OVERALL CASCADE FLOW FIELD

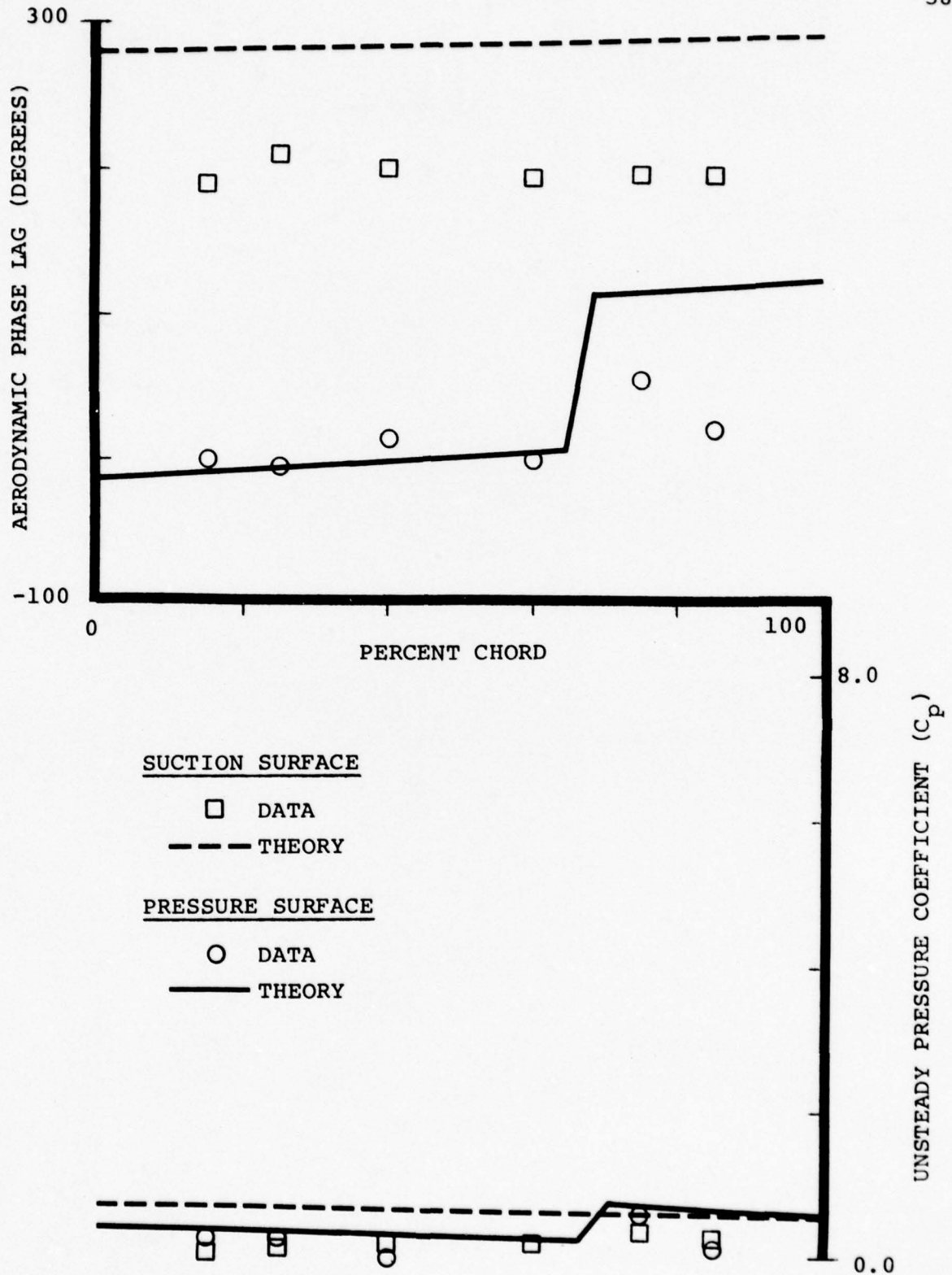


FIGURE 10. UNSTEADY CASCADE TRANSLATION MODE RESULTS FOR A 2.9° INTERBLADE PHASE ANGLE AT A STATIC PRESSURE RATIO OF 1.00:1

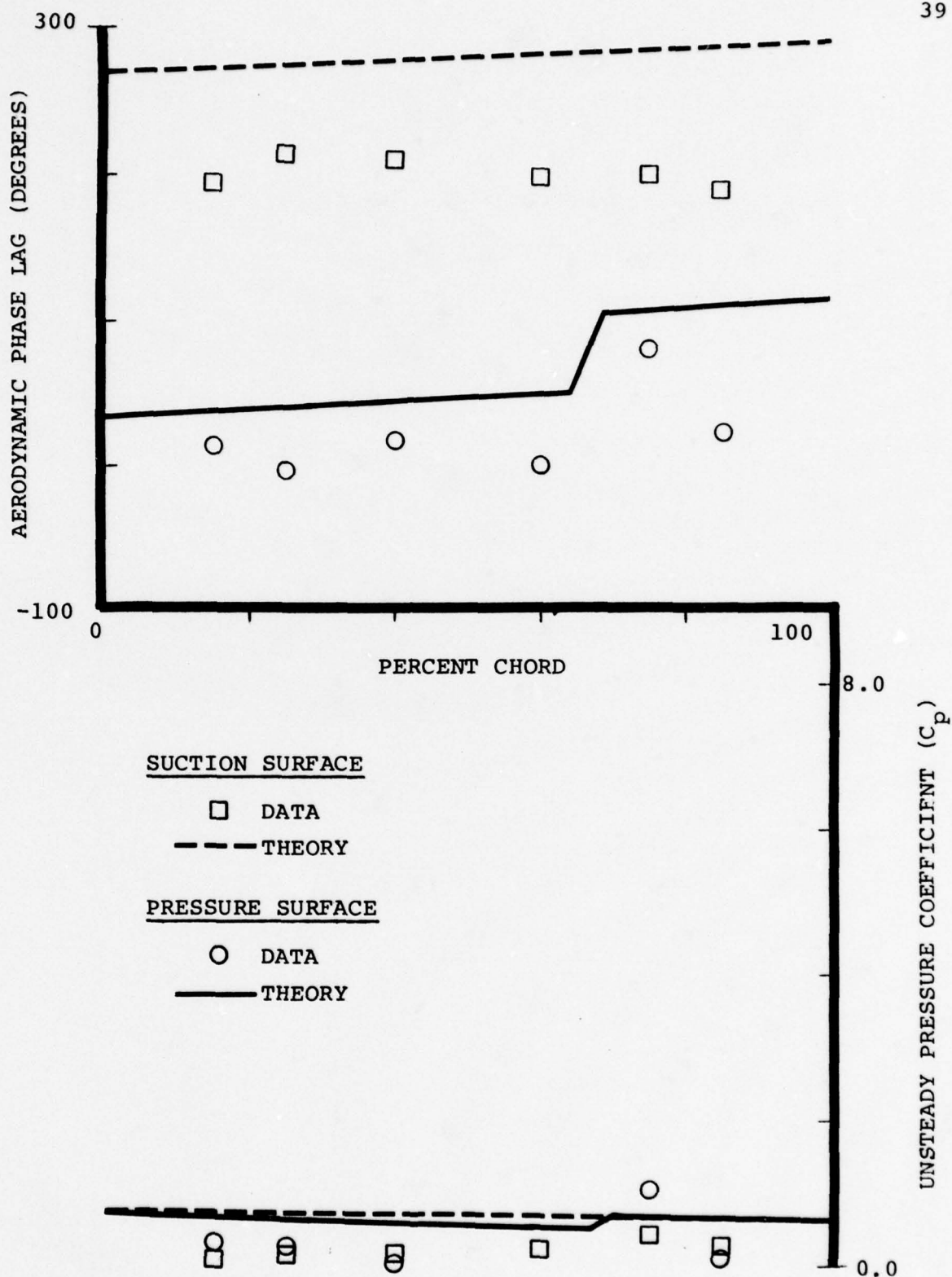


FIGURE 11. UNSTEADY CASCADE TRANSLATION MODE RESULTS FOR A -35.0° INTERBLADE PHASE ANGLE AT A STATIC PRESSURE RATIO OF 1.00:1

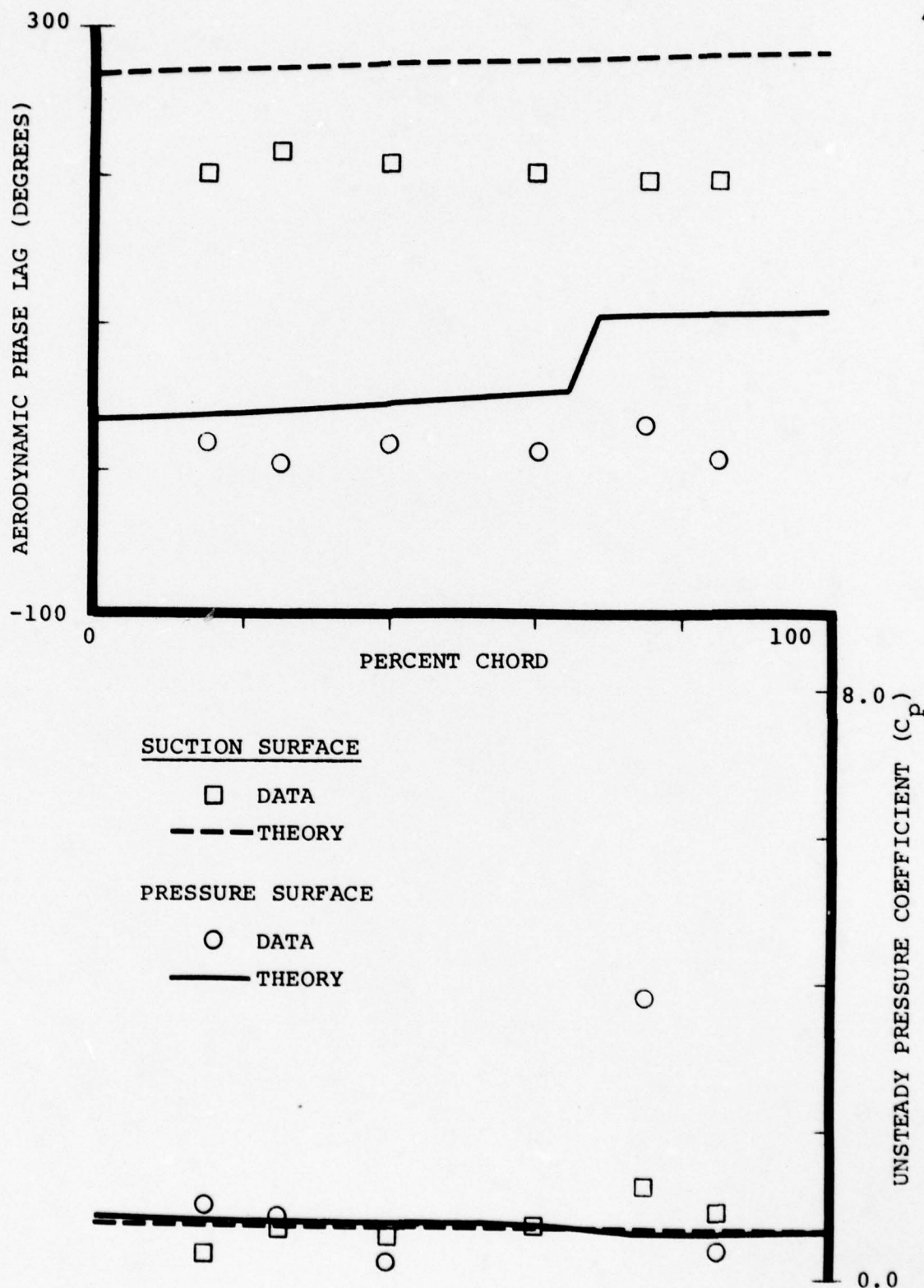


FIGURE 12. UNSTEADY CASCADE TRANSLATION MODE RESULTS FOR A -41.0° INTERBLADE PHASE ANGLE AT A STATIC PRESSURE RATIO OF 1.00:1

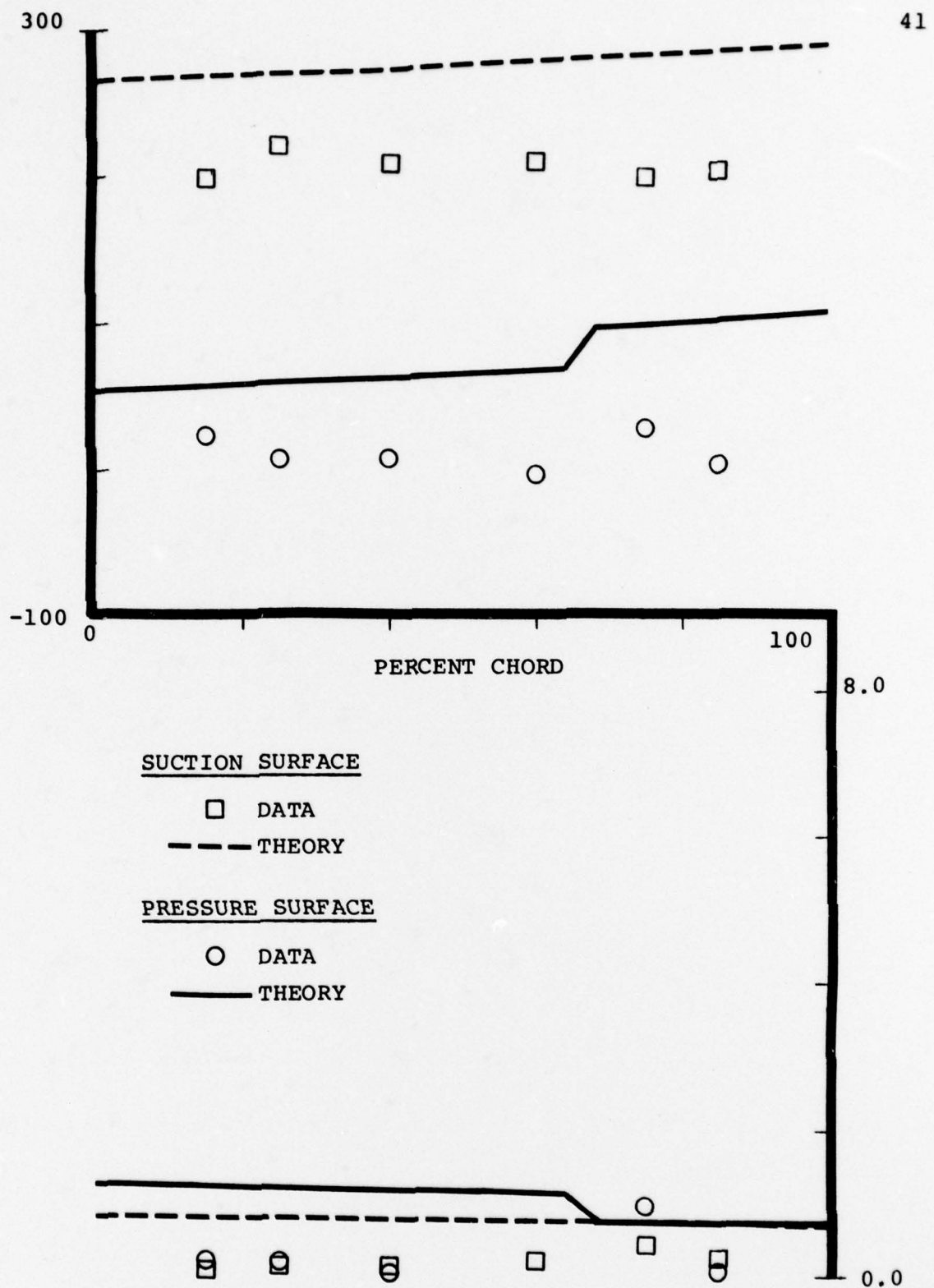


FIGURE 13. UNSTEADY CASCADE TRANSLATION MODE RESULTS
FOR A -90.0° INTERBLADE PHASE ANGLE AT A
STATIC PRESSURE RATIO OF 1.00:1

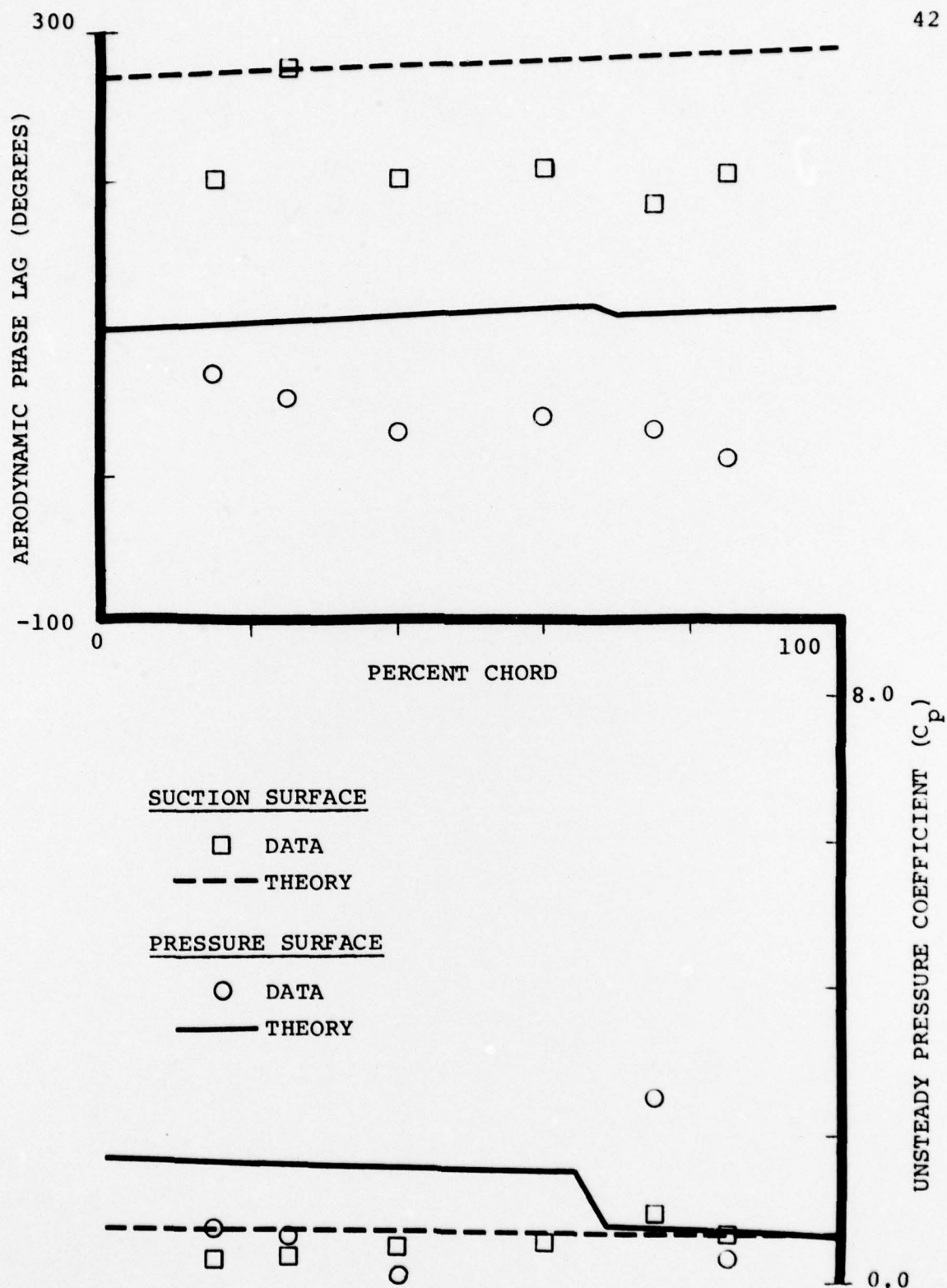


FIGURE 14. UNSTEADY CASCADE TRANSLATION MODE RESULTS
FOR A -178.0° INTERBLADE PHASE ANGLE AT A
STATIC PRESSURE RATIO OF 1.00:1

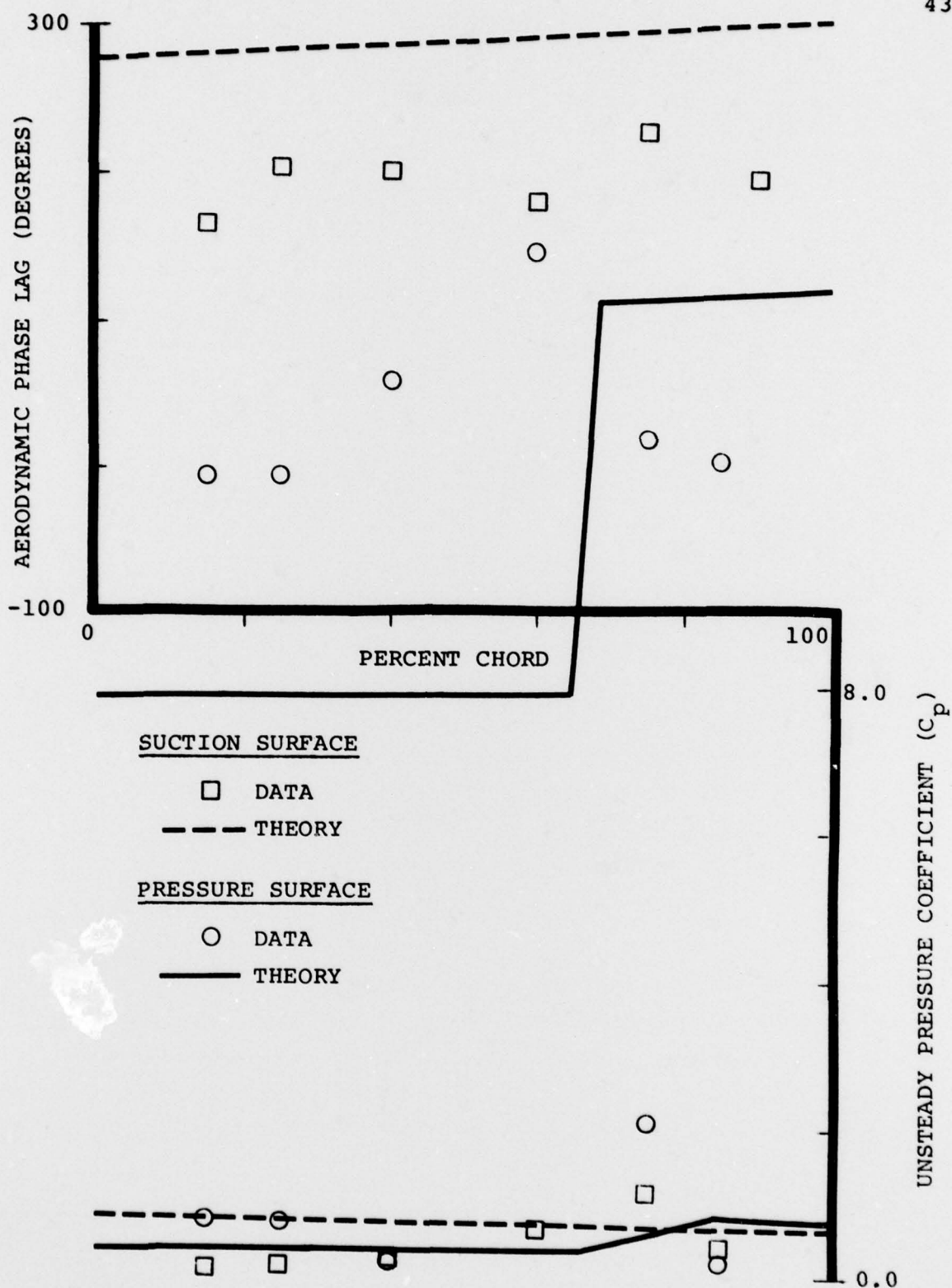


FIGURE 15. UNSTEADY CASCADE TRANSLATION MODE RESULTS FOR A 45.0° INTERBLADE PHASE ANGLE AT A STATIC PRESSURE RATIO OF 1.30:1

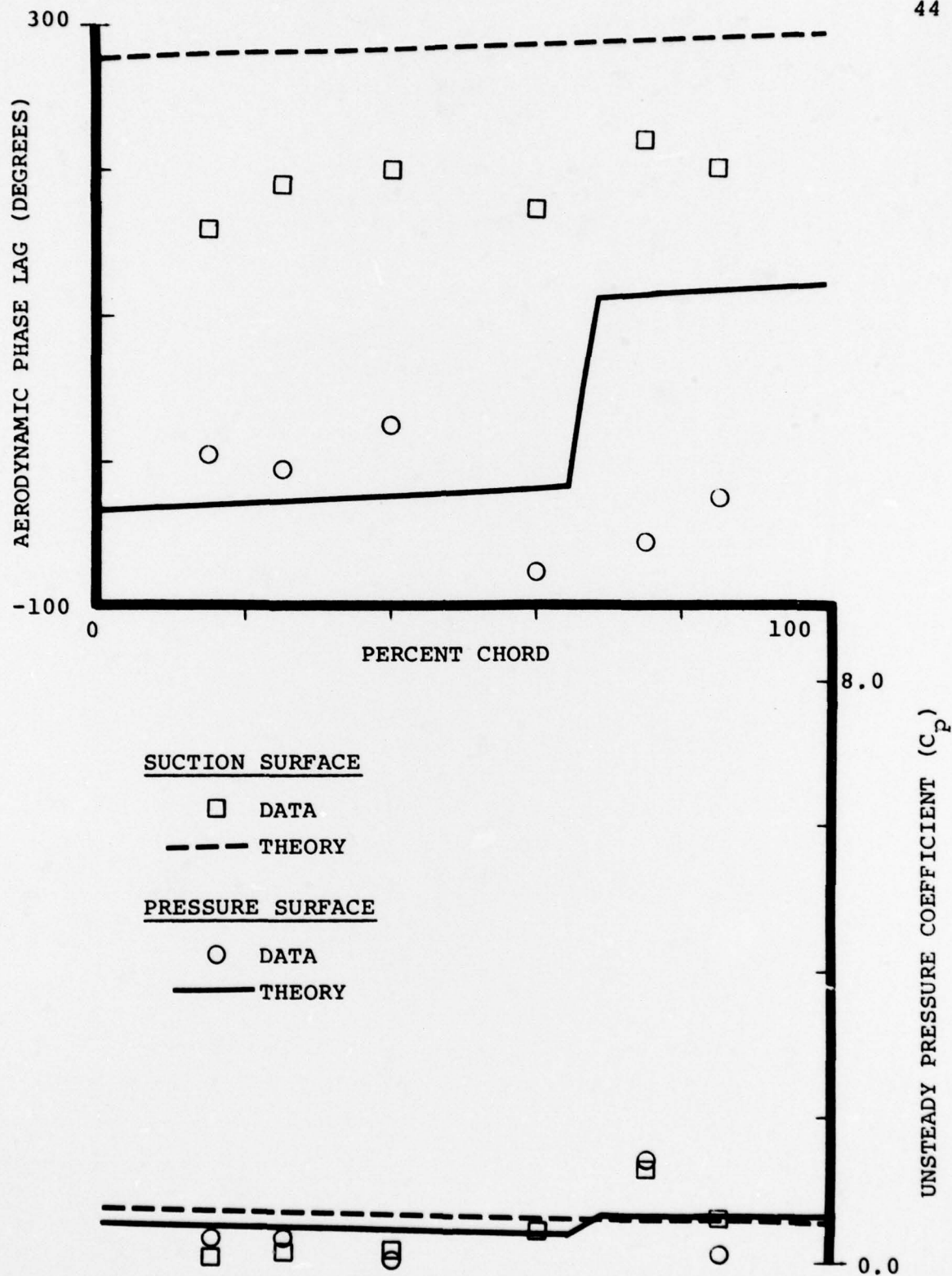


FIGURE 16. UNSTEADY CASCADE TRANSLATION MODE RESULTS FOR A 0.0° INTERBLADE PHASE ANGLE AT A STATIC PRESSURE RATIO OF 1.30:1

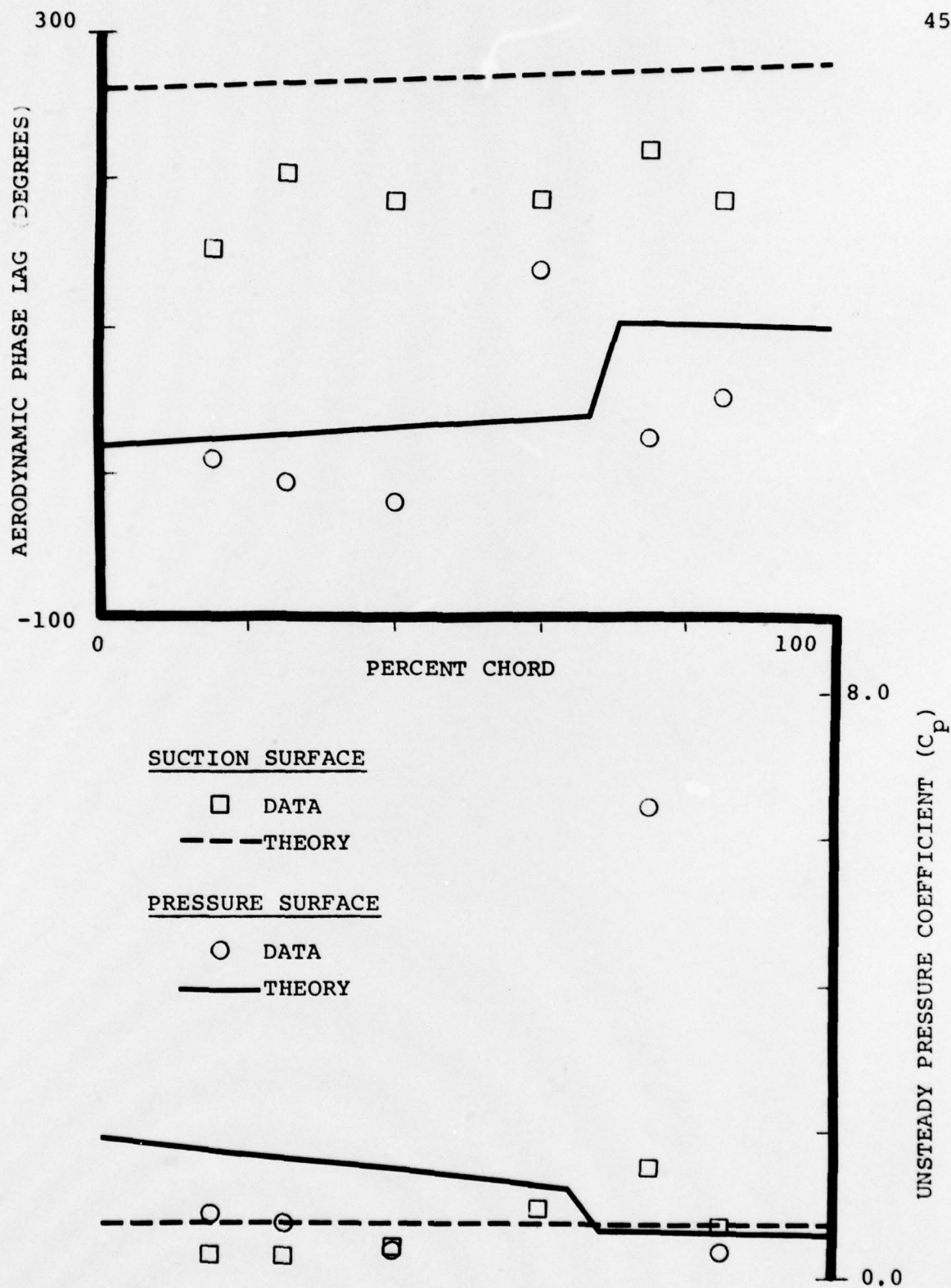


FIGURE 17. UNSTEADY CASCADE TRANSLATION MODE RESULTS
FOR A -64.0° INTERBLADE PHASE ANGLE AT A
STATIC PRESSURE RATIO OF 1.30:1

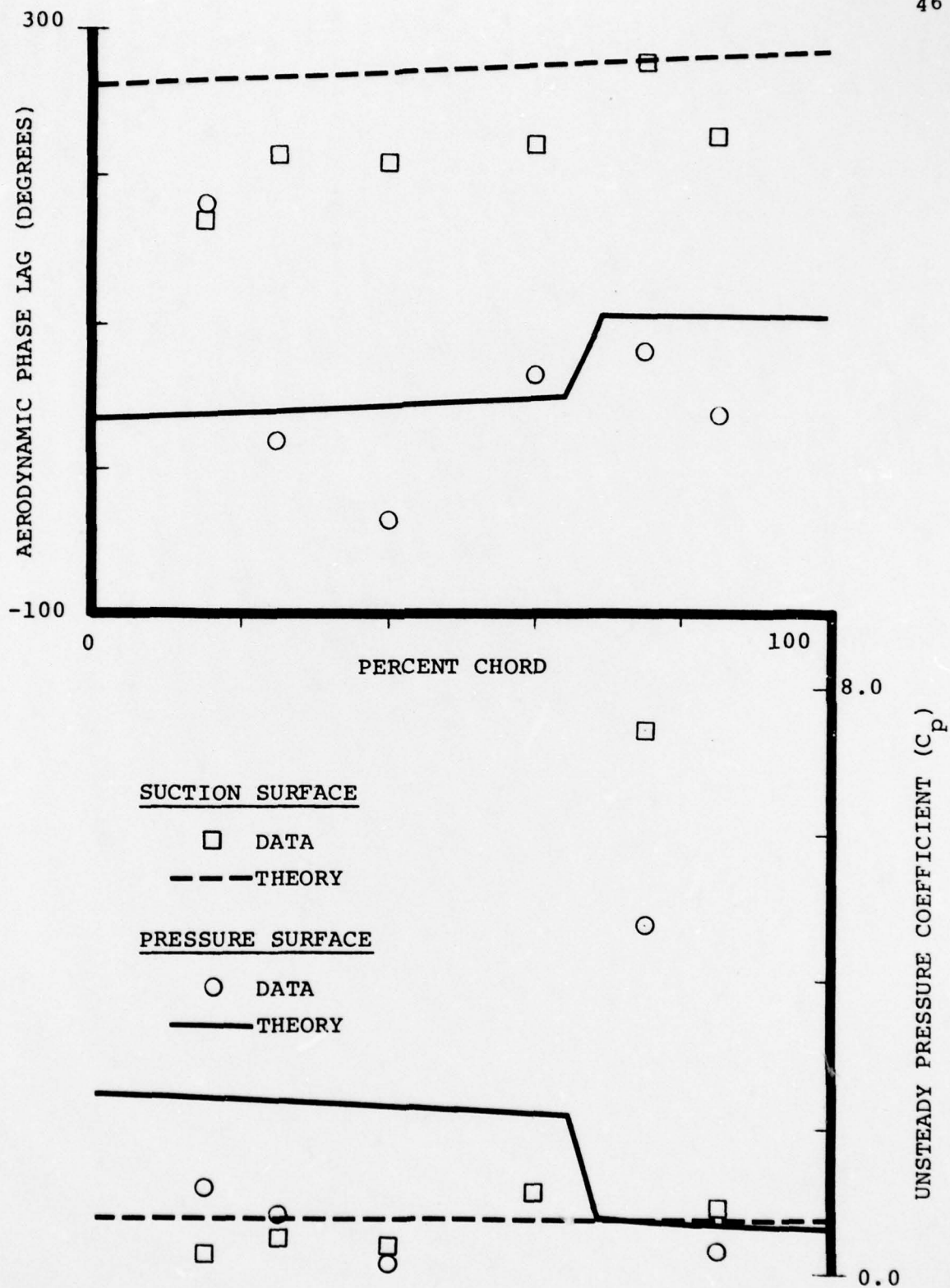


FIGURE 18. UNSTEADY CASCADE TRANSLATION MODE RESULTS FOR A -90.0° INTERBLADE PHASE ANGLE AT A STATIC PRESSURE RATIO OF 1.30:1

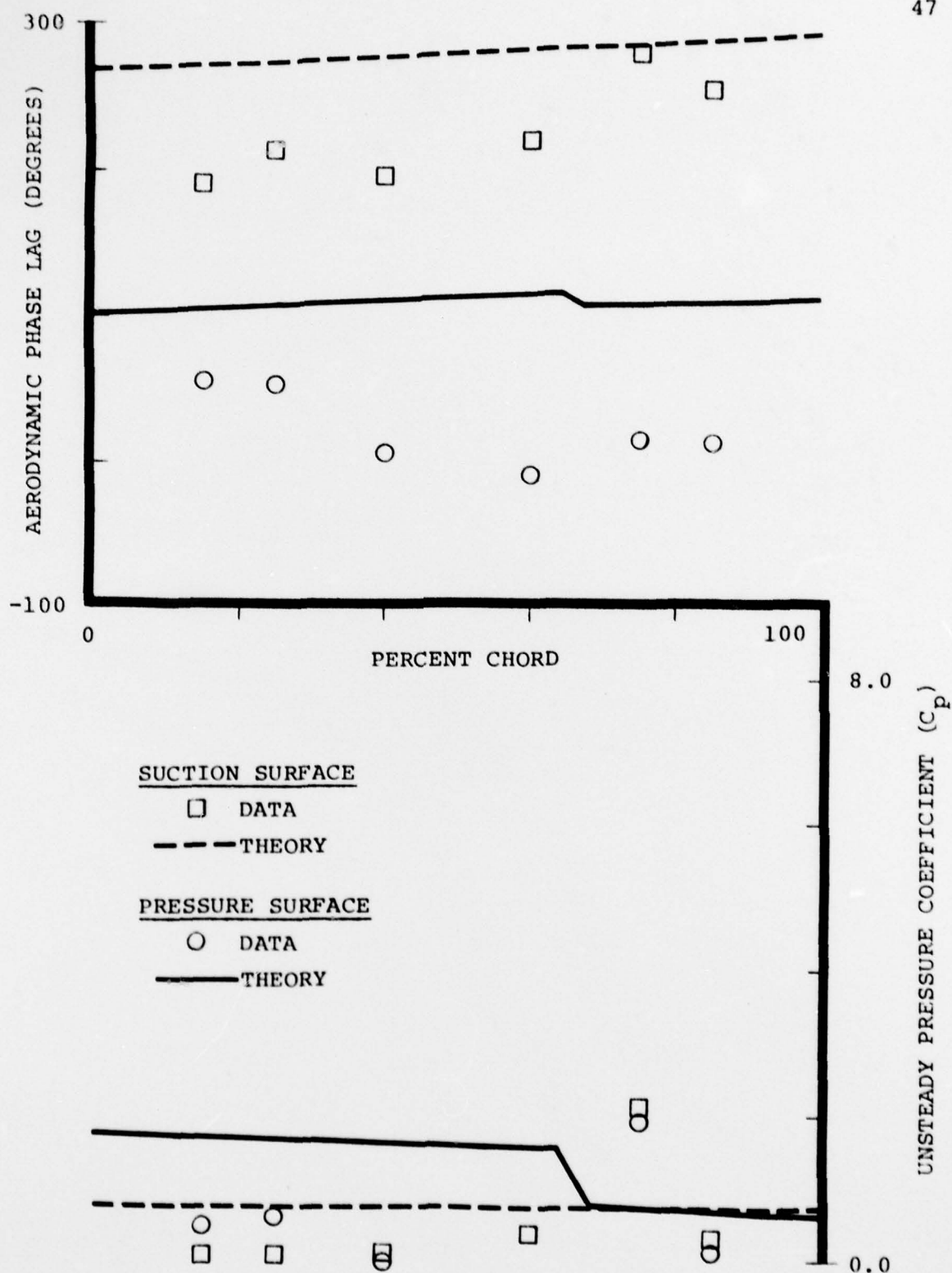


FIGURE 19. UNSTEADY CASCADE TRANSLATION MODE RESULTS FOR A -180.0° INTERBLADE PHASE ANGLE AT A STATIC PRESSURE RATIO OF 1.30:1

<u>Recipient</u>	<u>No. of Copies</u>
Director Power Program Material Sciences Division Office of Naval Research Department of the Navy 800 North Quincy Street Arlington, Virginia 22217	(1)
Chief of Naval Research Department of the Navy Washington, D.C. 20360 Attn: Mr. J. R. Patton, Jr., Code 473	(1)
Director U.S. Naval Research Laboratory Washington, D.C. 20390 Attn: Library, Code 2029 (ONRL)	(6)
Director U.S. Naval Research Laboratory Washington, D.C. 20390 Attn: Technical Information Division	(6)
Defense Documentation Center Building 5 Cameron Station Alexandria, Virginia 22314	(12)
Commander Naval Air Systems Command Department of the Navy Washington, D.C. 20360 Attn: Mr. R. R. Brown, Code 53673 Mr. I. Silver, Code 330 Dr. H. Rosenwasser, Code 310C Technical Library Division, Code 604	(1) (1) (1) (1)

<u>Recipient</u>	<u>No. of Copies</u>
Commander Naval Ship Systems Command Department of the Navy Washington, D.C. 20360 Attn: Mr. R. R. Peterson, Code 03413	(1)
Mr. C. Miller, Code 6146	(1)
Technical Library	(1)
 Commanding Officer U.S. Army Research Office Box CM, Duke Station Durham, North Carolina 27706 Attn: ORDOR-PC	(1)
 Director National Aeronautics and Space Administration Headquarters Washington, D.C. 20546 Attn: Division Research Information	(1)
 Office of the Assistant Secretary of Defense (R & D) Room 3E1065 - The Pentagon Washington, D.C. 20301 Attn: Technical Library	(1)
 General Motors Corporation Allison Division Indianapolis, Indiana 46206 Attn: Director of Engineering	(1)
 National Aeronautics and Space Administration Lewis Research Center 21000 Brookpark Road Cleveland, Ohio 44135	(2)
 Commander U.S. Naval Ordnance Laboratory White Oak Silver Spring, Maryland 20910 Attn: Library	(1)

<u>Recipient</u>	<u>No. of Copies</u>
Commander Naval Weapons Center China Lake, California 93555 Attn: Technical Library	(1)
Commander Wright Air Development Center Wright-Patterson Air Force Base, Ohio 45433 Attn: WCLPN-1, WCACD, WCLPS-1	(3)
Officer in Charge Naval Ship Engineering Center Philadelphia Division Philadelphia, Pennsylvania 19112 Attn: Code 6700 Technical Library	(1) (1)
Superintendent U.S. Naval Postgraduate School Monterey, California 93940 Attn: Professor Vavra Library, Code 0212	(1) (1)
Commander Naval Ordnance Systems Command Department of the Navy Washington, D.C. 20360 Attn: Mr. B. Drimmer, Code 033	(1)
Naval Ship Research and Development Center Annapolis, Maryland 21402 Attn: Library, Code A214	(1)
Naval Undersea Warfare Center 3202 East Foothill Boulevard Pasadena, California 91107 Attn: Technical Library	(1)
Naval Applied Science Laboratory Flushing and Washington Avenues Brooklyn, New York 11251 Attn: Technical Library, Code 222	(1)

<u>Recipient</u>	<u>No. of Copies</u>
Bureau of Naval Personnel Department of the Navy Washington, D.C. 20370 Attn: Technical Library	(1)
U.S. Naval Weapons Laboratory Dahlgren, Virginia 22448 Attn: Technical Library	(1)
Director, Project SQUID Jet Propulsion Center School of Mechanical Engineering Purdue University Lafayette, Indiana 47907 Attn: Dr. Robert Goulard	(1)
Army Missile Command Research and Development Directorate Redstone Arsenal, Alabama 35809 Attn: Propulsion Laboratory	(1)
Commander U.S. Air Force Systems Command Andrews Air Force Base Silver Hill, Maryland 20331	(1)
Commander Air Force Aero Propulsion Laboratory Wright-Patterson Air Force Base Dayton, Ohio 45433	(1)
Commander Air Force Rocket Propulsion Laboratory Edwards Air Force Base, California 93523	(1)
Naval Missile Center Point Mugu, California 93041 Attn: Technical Library Code 5632.2	(1)

<u>Recipient</u>	<u>No. of Copies</u>
Headquarters Naval Material Command Special Projects Office Washington, D.C. 20360 Attn: Technical Library	(2)
Commander Air Force Office of Scientific Research 1400 Wilson Boulevard Arlington, Virginia 22209 Attn: J. F. Masi M. Rogers	(1)
Director of Defense Research and Engineering Technical Library Room 3C128 - The Pentagon Washington, D.C. 20301 Attn: Propulsion Technology	(1)
Chief of Research and Development Headquarters, Department of the Army Washington, D.C. 20310 Attn: Dr. S. J. Magram Physical and Engineering Division	(1)

UNCLASSIFIED

SECURITY CLASSIFICATION OF THIS PAGE (When Data Entered)

REPORT DOCUMENTATION PAGE		READ INSTRUCTIONS BEFORE COMPLETING FORM
1. REPORT NUMBER 24 EDR-9477	2. GOVT ACCESSION NO.	3. RECIPIENT'S CATALOG NUMBER
4. TITLE (and Subtitle) 6 Research on Aeroelastic Phenomena in Airfoil Cascades; An Experimental Investigation of the Unsteady Aerodynamics of a Classical Airfoil Cascade in Translation.	5. TYPE OF REPORT & PERIOD COVERED 9 Technical Report	
7. AUTHOR(s) 24 Sanford/Fleeter, Ronald E./Riffel, Thomas H. Lindsey, Mark D./Rothrock	6. PERFORMING ORG. REPORT NUMBER	
9. PERFORMING ORGANIZATION NAME AND ADDRESS Detroit Diesel Allison Division General Motors Corporation Indianapolis, Indiana 46206	8. CONTRACT OR GRANT NUMBER(s) 15 N00014-72-C-0351	
11. CONTROLLING OFFICE NAME AND ADDRESS Power Branch Office of Naval Research - Code 473 Arlington, Virginia 22217	10. PROGRAM ELEMENT, PROJECT, TASK AREA & WORK UNIT NUMBERS NR 094-369	
14. MONITORING AGENCY NAME & ADDRESS (if different from Controlling Office)	12. REPORT DATE 11 April 1978	
	13. NUMBER OF PAGES 61 22 54p.1	
	15. SECURITY CLASS. (of this report) Unclassified	
15a. DECLASSIFICATION DOWNGRADING SCHEDULE		
16. DISTRIBUTION STATEMENT (of this Report) This document has been approved for public release and sale; its distribution is unlimited.		
17. DISTRIBUTION STATEMENT (of the abstract entered in Block 20, if different from Report)		
18. SUPPLEMENTARY NOTES		
19. KEY WORDS (Continue on reverse side if necessary and identify by block number) Flutter, Aeroelasticity, Turbomachinery, Aerodynamics, Experimental Techniques, Cascades, Dynamic Measurements		
20. ABSTRACT (Continue on reverse side if necessary and identify by block number) The advent of high tip-speed, high work, blading in the fan stages of advanced gas turbine engines has led to the recognition of a new type of blading instability - unstalled supersonic flutter. As a result, a concerted effort to develop an appropriate predictive mathematical model has taken place. To determine the range of validity and to direct refinements to the basic flow model, fundamental supersonic oscillating cascade data are required. The		

DD FORM 1 JAN 73 1473

EDITION OF 1 NOV 65 IS OBSOLETE

UNCLASSIFIED

SECURITY CLASSIFICATION OF THIS PAGE (When Data Entered)


019 200

rest
Page
hh

UNCLASSIFIED

SECURITY CLASSIFICATION OF THIS PAGE(When Data Entered)

experiment described herein is directed at significantly extending the range of existing supersonic cascade data to include translation mode oscillations. In particular, the fundamental time-variant translation mode aerodynamics are determined for the first time for a classical airfoil cascade in a supersonic inlet flow field over a range of interblade phase angles at a realistic reduced frequency value. These unique experimental data are then correlated with predictions obtained from an appropriate state-of-the-art harmonically oscillating flat plate cascade aerodynamic analysis.



UNCLASSIFIED

SECURITY CLASSIFICATION OF THIS PAGE(When Data Entered)